analytical chemistry

Article

pubs.acs.org/ac

How Actuated Particles Effectively Capture Biomolecular Targets

Alexander van Reenen,[†,‡,∥] Arthur M. de Jong,[†,‡] and Menno W. J. Prins*[,†,‡,§]

[†]Department of Applied Physics, [‡]Institute for Complex Molecular Systems, [§]Department of Biomedical Engineering, Eindhoven University of Technology, 5600 MB Eindhoven, The Netherlands

Supporting Information

ABSTRACT: Because of their high surface-to-volume ratio and adaptable surface functionalization, particles are widely used in bioanalytical methods to capture molecular targets. In this article, a comprehensive study is reported of the effectiveness of protein capture by actuated magnetic particles. Association rate constants are quantified in experiments as well as in Brownian dynamics simulations for different particle actuation configurations. The data reveal how the association rate depends on the particle velocity, particle density, and particle assembly characteristics. Interestingly, single particles appear to exhibit target depletion zones near their surface, caused by the high density of capture molecules. The depletion effects are even more limiting in cases with high particle densities. The depletion effects are overcome and protein capture rates are enhanced by applying dynamic particle actuation, resulting in an increase in the association rate constants by up to 2 orders of magnitude.

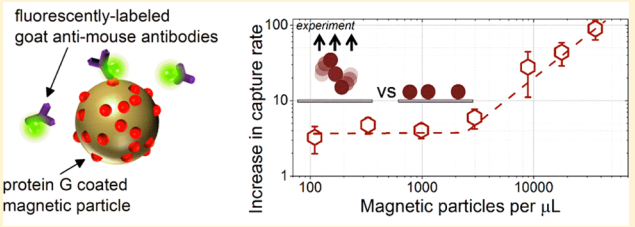

Particle-based techniques are widely exploited in bioanalysis[1] and clinical diagnostics[2] for extracting target substances from a biological matrix based on either generic physicochemical capture principles[3,4] or biologically specific capture. The binding of biomolecular targets to a single particle or a single cell has been a topic of study for several decades due to its relevance for bioanalysis and cellular processes. Pickard[5] published an extensive overview of existing theories and models for molecular transport to or from a particle. The transition from target transport dominated by diffusion to transport dominated by advection is described by the dimensionless Péclet number, $Pe = L \cdot v/D$, where L is a characteristic length scale of the system, v is the velocity of the particle, and D is the diffusion constant of the target molecules. Pickard concluded that almost all reported studies involved theoretical considerations and that no relevant experimental studies were reported in the biologically interesting region of Péclet numbers between 0.1 and 10.

Magnetic particles have the advantage that their velocities can be carefully controlled by magnetic fields.[6,7] Furthermore, their actuation properties can be used to effectuate series of processing steps in a diagnostic assay,[7] such as buffer exchange, washing, concentration, transportation and dispersion,[8] and labeling. By combining various steps, complete assays can be integrated in a lab-on-chip testing device. These processes exploit the high surface-to-volume ratio and adaptable surface functionalization of particles. For a given surface functionalization, the effectiveness and rate of target capture critically depend on the way the particles and fluid are brought into contact with each other and on the amount of particles used. The capture rate scales with the amount of particles, but it saturates when the particles themselves start to hinder the target capturing process. Magnetic actuation has been frequently presented as a means to speed up biochemical reactions,[7] but the exact influence of actuation on the capture processes has not been clearly reported.

In this article, we investigate in detail the effectiveness of biomolecular target capture by single particles and by ensembles of particles, with the aim to understand and resolve the key limiting factors. The effectiveness of capture was studied in a model assay with protein G-coated magnetic particles and fluorescently labeled antibodies as targets (Figure 1). We find that even single particles have a target depletion zone near their surface, which leads to a reduced capture rate. The depletion effects become even more limiting for high particle densities. We demonstrate that the depletion effects can be overcome by actuating the particles through the fluid, using gravitational or magnetic forces. We summarize the findings in terms of actuation principles and dimensionless numbers that will help in the design of efficient and rapid particle-based capture processes for the generation of novel, highly sensitive, and miniaturized lab-on-chip biosensing systems.

MATERIALS AND METHODS

Model System for Particle-Based Target Capture. Magnetic particles (ø2.8 μm, carboxylated M270, Dynal Biotech) were coated covalently with recombinant protein G (Thermo Scientific) using standard EDC-NHS coupling chemistry. As targets, we used goat anti-mouse IgG antibodies labeled with Alexa Fluor 488 dye (Invitrogen). Both the particles and target antibodies were diluted in assay buffer, i.e., phosphate buffered saline containing 0.1% bovine serum

Received: October 14, 2016
Accepted: February 13, 2017
Published: February 13, 2017

DOI: 10.1021/acs.analchem.6b04043
Anal. Chem. 2017, 89, 3402−3410

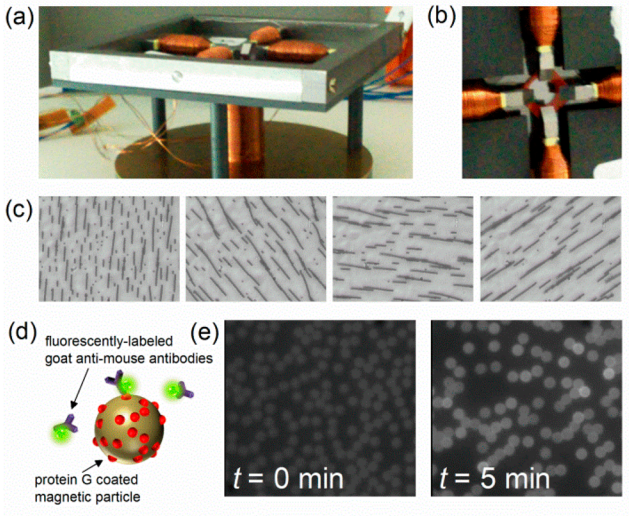

Figure 1. Experiment for studying particle-based target capture by actuated magnetic particles. (a) Magnetic fields were generated by a five-pole electromagnet containing soft iron parts to concentrate field lines at its center (b) where the disk-shaped 38 μL incubation chamber was located. (c) Microscope top-view images of rotating chains of magnetic particles. (d) The experimental model system to study the capture process. (e) Fluorescence microscopy images of particles before and after target capture. The average fluorescence of the particles was compared to the background to quantify the capture of targets. Due to autofluorescence, the particles are already visible at $t = 0$.

albumin (BSA; Merck) and 0.02% Tween-20 (Thermo Scientific).

To quantify the maximum binding capacity of the magnetic particles, we performed a supernatant assay in which magnetic particles ($\sim 9 \times 10^6$ particles/μL) were incubated with ~60 nM antibodies for 3 h. After a magnetic washing step, we measured the fluorescence of the supernatant using a Fluoroskan Ascent FL. Compared to a control in which no magnetic particles were incubated, a 4.4 ± 0.3% decrease was found in the fluorescence signal, from which we calculate that a single magnetic particle can bind $(1.8 \pm 0.2) \times 10^5$ antibodies.

Preparation and Filling of the Incubation Chamber. Microfluidic incubation chambers were shaped as a flat cylinder (Figure 2b). The chambers were made by attaching adhesive Secure-Seal hybridization chambers (⌀9 mm, height = 0.6 mm; Electron Microscopy Sciences) to a glass coverslip (VWR) that was cleaned beforehand using isopropanol. On the nonadhesive side, the hybridization chambers had a 0.25 mm thick polycarbonate sheet containing two inlets to fill the 38 μL incubation chamber. The sheet was transparent to allow imaging from this side using a microscope (Leica DM6000). Prior to an experiment, the incubation chamber was filled with assay buffer (containing no particles or targets) in order to block the chamber with BSA and thereby minimize nonspecific adhesion.

In experiments, a 4 μL magnetic particle suspension (2×10^5 particles/μL; unless stated otherwise) was dispensed in the incubation chamber. After 1 min (to allow the particles to sediment to the bottom surface), the incubation chamber was filled with the target solution (~34 μL with a concentration of 110 pM; unless stated otherwise). To prevent evaporation losses, the chamber was sealed using adhesive port seals as supplied together with the hybridization chambers.

Magnetic Field Generation. To generate time-dependent magnetic fields in the incubation chamber, an electromagnet setup was designed and built consisting of five electromagnets (Figure 1a,b). The setup consists of a quadrupole electromagnet (800 windings with ⌀0.25 mm copper wires) to generate magnetic fields, oriented in-plane with respect to the bottom surface of the incubation chamber. A separate electromagnet (1600 windings with ⌀0.25 mm copper wires) was positioned below the center of the quadrupole electromagnet to allow for the generation of fields oriented out-of-plane. With the quadrupole electromagnet, magnetic fields can be generated that rotate in-plane with respect to the incubation chamber (Figure 1c), whereas by combining the bottom electromagnet with two opposite electromagnets of the quadrupole, magnetic fields can be generated that rotate out-of-plane. To guide field lines to the incubation chamber, soft iron parts were implemented in the setup.

The electromagnets were powered using a controller that was steered using LabView software to allow for the application of actuation protocols to each coil separately, which can vary in time in terms of the amplitude, frequency, and waveform (i.e., sinusoidal) of the current. The calibration of the magnetic field was performed using a Gauss meter (5100 series F.W. Bell); the data can be found in Supporting Information S1.

Magnetic Redispersion of Particles after Actuation. After the application of each actuation sequence, particles were actively disaggregated and redistributed over the bottom surface by means of a method called magnetic interfacial rotaphoresis (see Supporting Information S2 and ref 8). Interfacial rotaphoresis allowed us to microscopically evaluate all particles because they were evenly spread over the surface.

Quantification of Target Capture. To quantify target capture for different types of actuation, we monitored the fluorescence intensity of the particles. Before actuation and after the application of a single actuation protocol, the incubation chamber was placed under a microscope (Leica DM6000). Using a water immersion objective lens (63×), the bottom surface with particles was imaged at a final magnification of 630×. The redistributed particles stayed on the bottom surface by gravitational forces. Excitation light (λ = 480 ± 20 nm) was generated by an external light source (Leica EL6000) combined with a L5 (Leica) filter cube. Fluorescence (within the range of λ = 527 ± 15 nm) was recorded using an EMCCD camera (Andor Luca S). For each measurement, images were taken from three random locations (with a field of view of 142 × 107 μm^2). After a measurement, the incubation chamber was placed back into the electromagnet setup to start the next actuation sequence.

Images (Figure 1e) were processed using ImageJ software (http://rsbweb.nih.gov/ij/) and Matlab (Mathworks) to determine the average fluorescence intensity of the particles with respect to the background intensity. The method is discussed in more detail in Supporting Information S3. We verified that antibody capture was specific, as presented in Supporting Information S4.

RESULTS AND DISCUSSION

First, we present two brief theoretical considerations to illustrate how particle actuation can increase the target capture rate. The first consideration treats advective replenishment in absence of diffusion. The second consideration deals with diffusive transport. Basically, magnetic actuation causes particles to move through the fluid and thereby displace fluid volume

DOI: 10.1021/acs.analchem.6b04043
Anal. Chem. 2017, 89, 3402−3410

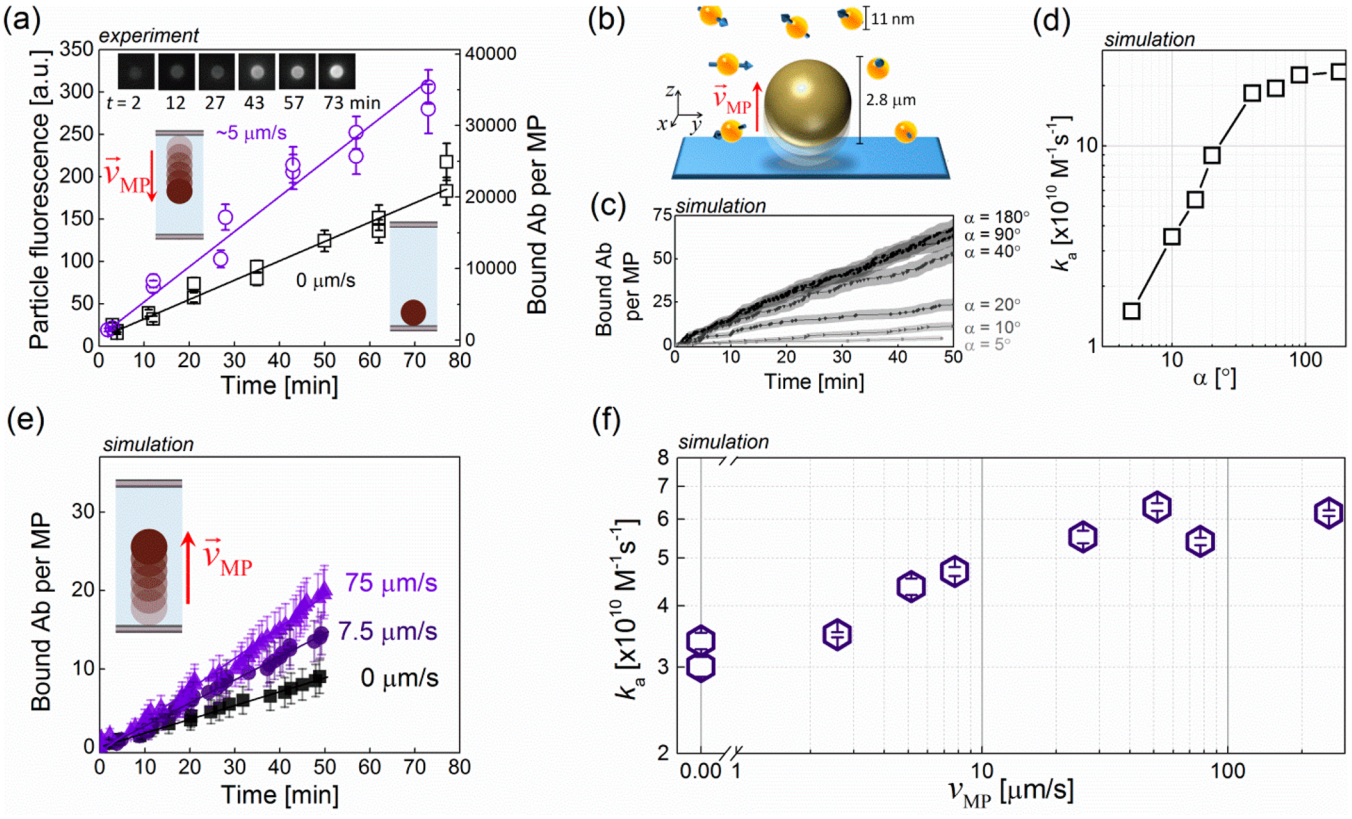

Figure 2. Experiment and simulations on target capture by linear translation of single particles. (a) Capture of fluorescently labeled antibodies (110 pM). The particles were moved through the incubation chamber by gravitational forces (see inset illustration) by reversing the chamber every 2 min, leading to an estimated particle sedimentation velocity of 5.1 μm/s. The inset shows fluorescence microscope images of particles at different incubation times. The number of bound antibodies per magnetic particle is indicated on the right axis. The solid lines correspond to least-squares linear fits to the data. (b) Schematic overview of the system simulated by Brownian dynamics, showing the magnetic capture particle (brown) and the target particles (orange). (c) Simulated capture of antibodies for varying binding range α of the targets (values for α are shown on the right). The target concentration was 0.1 pM. (d) Association rate constants as determined from linear fits to the data in panel c. (e) Simulated capture for different particle velocities and for $\alpha = 10°$. The inset shows that particles start at the bottom and then move up and down through the fluid. (f) Association rate constants as a function of the particle velocity, determined from linear fits to the data in panel e.

elements. Let us assume a single magnetic particle with diameter d that translates linearly with velocity v through a static fluid. Due to its cross-section, the particle displaces a fluid volume V per unit time that can be approximated by

$$\frac{dV}{dt} = v\frac{1}{4}\pi d^2 \tag{1}$$

This gives a number of displaced target molecules N_{displ} per unit time

$$\frac{dN_{displ}}{dt} = C_{target}\frac{dV}{dt} = C_{target}\frac{1}{4}\pi d^2 v \tag{2}$$

with C_{target} being the concentration of targets in the fluid. The target capture rate is related to the number of capture molecules immobilized on the particle (N_{CM}), the association rate constant of the individual capture molecules (k_{on}), and the local concentration of targets at the particle surface. When there is no depletion of targets, the capture rate onto a single particle is given by

$$\frac{dN_{capt}}{dt} = k_{on}N_{CM}C_{target} = k_{on}\sigma\pi d^2 C_{target} \tag{3}$$

with σ being the areal density of capture molecules on the particle surface. We assume that target capture is effectuated without depletion limitation when the number of targets displaced per unit of time is larger than the number of targets captured per unit time, i.e., $dN_{displ}/dt > dN_{capt}/dt$. Using eqs 2 and 3, we find the following expression for the minimum velocity to avoid depletion

$$v_{no\text{-}depl} = 4k_{on}\sigma \tag{4}$$

Using this relation, we can estimate whether a reaction is limited by local depletion of targets near the particles or not. The velocity minimum to avoid depletion limitation scales with the reaction rate constant and the areal density of capture molecules on the particle surface. This is expected as both these factors determine the rate at which targets are captured. Interestingly, the limit is independent of the particle size as both the target displacement and capture processes scale with the particle size. We can now estimate the particle velocity necessary for particle-based target capture without depletion limitation. Using a relatively low surface density of capture molecules [$\sigma = 1/(100\text{ nm})^2 = 10^{14}$ m^{-2}] and a common value for the association rate per capture molecule [$k_{on} = 10^5$ M^{-1} s^{-1} $= 1/6 \times 10^{-21}$ m^3/s],[9] we find a velocity of $v_{no\text{-}depl} > 100$ μm/s. This velocity is relatively high, so from these estimations, we can expect that depletion effects should indeed be visible in particle-based capture experiments without actuation.

DOI: 10.1021/acs.analchem.6b04043
Anal. Chem. 2017, 89, 3402−3410

When target depletion occurs near a linearly translating capture particle, then the depletion zone is nonspherical, with the strongest depletion being present at the wake-side of the particle. At low particle velocities, the transport of targets across the local concentration gradient is dominated by diffusion, and at high velocities, the transport is dominated by advection. Advective transport dominates over diffusive transport when $Pe > 1$, i.e.

$$v_{\mathrm{adv>diff}} > D/d \tag{5}$$

Using this relation, a particle velocity can be estimated to allow advective transport to dominate over diffusive transport. We use a particle diameter of 2.8 μm, and we compute the diffusion constant using the Stokes−Einstein relation (T = 293 K) with a target hydrodynamic radius of ∼5.5 nm, corresponding to IgG.[10] On the basis of this input, we find a velocity of $v_{\mathrm{adv>diff}} \sim 10$ μm/s.

Pickard[5] made a mathematical analysis on the flux enhancement due to convective flow of reactant to an ideally absorbing sphere. He derived relations for the flux enhancement relative to the flux expected from pure diffusion as a function of Péclet number. The above-mentioned velocity of 10 μm/s corresponds to a Péclet number equal to 1. According to Pickard, the relative flux enhancement relative to a nonmoving sphere is in the range of 100% for conditions in the vicinity of $Pe \approx 1$.

From the above theoretical estimations, we conclude that depletion effects may indeed appear in particle-based capture experiments without actuation and that advective transport due to particle actuation may resolve the limitations imposed by diffusion.

Target Capture by Actuated and Nonactuated Single Particles. First, we discuss target capture and depletion effects in the limit of single particles. We studied the capture rate of magnetic particles at very low particle concentrations (100 particles/μL). The amount of captured targets on the particle surface was quantified by measuring the average particle fluorescence signal during the incubation process (see Figure 1e and Supporting Information S3 and S4). We compared the capture of targets on the one hand for particles lying on a surface and on the other hand for particles linearly translating through a fluid due to gravitational forces by repeatedly turning the fluid cell upside down. In Figure 2a, the measured fluorescence intensity is shown for both experiments. The induced particle velocity of v_{MP} = 5.1 μm/s was estimated by balancing the Stokes drag with the gravitational force on a single particle: $6\pi\eta R_{\mathrm{MP}} v_{\mathrm{MP}} = 4\pi R_{\mathrm{MP}}^3 (\rho_{\mathrm{MP}} - \rho_{\mathrm{medium}}) g$. Comparing both cases, it is found that the capture rate is increased by a factor of 1.9 ± 0.1 when particles translate through the fluid compared to static particles.

Using these results as a reference, we numerically modeled the capture process using Brownian dynamics. The specific details of the method are described in Supporting Information S8. Basically, as sketched in Figure 2b, we simulated a magnetic particle at different translational velocities within a rectangular fluid cell with a height equal to the incubation chamber. The width of the fluid cell was set at 100 μm, and periodic boundary conditions were used at the sides. This corresponds to the average particle distance in the experiment. Target antibodies were modeled as spherical particles with a hydrodynamic radius of ∼5.5 nm.[13] Initially, target particles are randomly distributed, and we compute their random displacement and rotation due to Brownian motion as well as hydrodynamic interactions due to the movement of the magnetic particle through the fluid. Interactions between the target particles were neglected because the target concentrations were very low. The capture process is modeled by treating the boundary of the magnetic particle as being partially absorbing. Specifically, binding is assumed only for angular differences smaller than a predefined angle $\alpha \in [0, \pi]$ between (i) the orientation vector of the target and (ii) the relative position vector between the particle and the target. In other words, the target needs to orient its binding site toward the magnetic particle in order to bind. Targets bind only for a limited range of orientations and otherwise reflect from the surface ($0 < \alpha < \pi$). For $\alpha = \pi$, targets always bind independent of their orientation. A numerical time step of 3 μs was chosen, which was found to be small enough to keep propagation errors negligible (see Supporting Information S8).

First, we simulated target capture by nonactuated magnetic particles (i.e., sedimented onto the surface) for different values for the binding range α. As shown in Figure 2c,d, the binding rate strongly depends on α, especially at low values. For a binding range of $\alpha \cong 10°$, similar association rate constants are found as in experiments (Figure 2a), i.e., 5×10^{10} M^{-1} s^{-1} (see Supporting Information S5). Note that the target concentrations are much lower in the simulations than in the experiments, by a factor of 1.1×10^3. An experiment at 0.1 pM would give approximately 12 targets bound to a single particle after 50 min. Compared to completely absorbing spheres, i.e., $\alpha = \pi$, the association rate constant for $\alpha \cong 10°$ is reduced by a factor of 7 ± 1. In the literature, it has been reported[9] that binding ranges of $\alpha \cong 5°$ lead to association rate constants similar to those found for free antibody−antigen association. The larger binding range that we find is possibly caused by the presence of multiple binding sites within close proximity on the surface of the magnetic particles. During an encounter with a particle, a target protein can interact with multiple binding sites, which is much less probable for a protein free in solution. The interaction with multiple binding sites effectively increases the allowed binding range for which the target can react.

Next, taking a binding range of $\alpha = 10°$, we simulated the effect of active particle translation through the sample volume. As shown in Figure 2e,f, we find that increased translation velocities enhance the capture rate. For a velocity as generated by gravitation, the obtained increase is a factor of 1.4 ± 0.2. These conditions for the translating particles correspond to $Pe \approx 0.4$. According to Pickard,[5] relative enhancements of up to 100% (factor 2) can be expected.

In the experiments, we even find an increase of 1.9 ± 0.3 (Figure 2a). Compared to the simulations, the experimental system exhibits (i) nonspherical targets, namely, antibodies that have a flexible structure allowing a dynamic configuration; (ii) magnetic particles with a surface roughness of about 10^1−10^2 nm in size (see Supporting Information S9); and (iii) specific interactions that may act on a longer range than hard-sphere collisions. These factors may influence the near-surface alignment process during the encounter between target and particle. Still, the increase of the motion-induced capture rate calculated from the simulation is close to the experimental values, showing that the enhancement in the capture rate can be at least partially understood from the physical transport processes of the particles and the targets in the fluid. We conclude that the particle motion generates more encounters between targets and particles and that, indeed, target depletion occurs near the particle's surface.

In the following sections, the capture process is studied for ensembles of capture particles rather than for isolated particles.

DOI: 10.1021/acs.analchem.6b04043
Anal. Chem. 2017, 89, 3402−3410

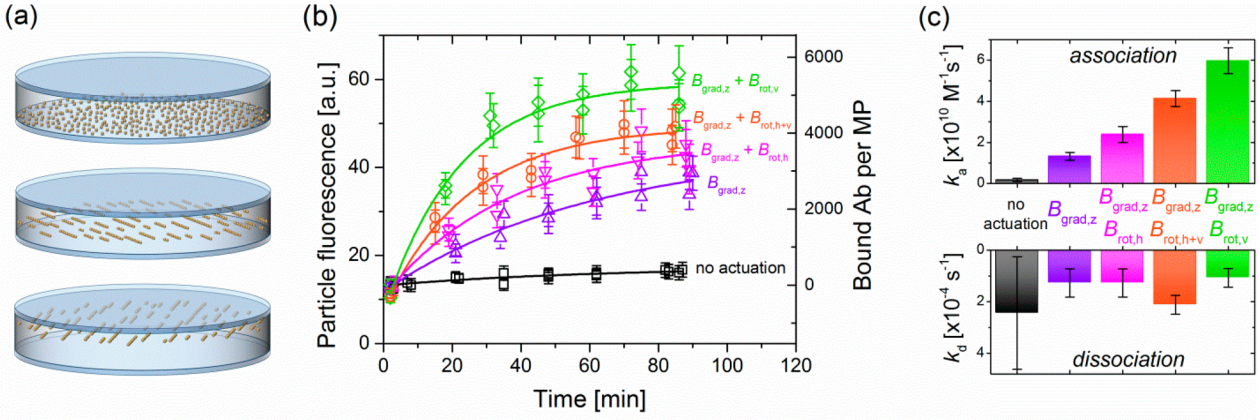

Figure 3. Experimental data on target capture by magnetically actuated ensembles of particles. Target capture was measured for different types of magnetic actuation: no actuation; only translation ($B_{grad,z}$); and translation combined with rotation in-plane ($B_{rot,h}$), out-of-plane ($B_{rot,v}$), or alternating in both directions ($B_{rot,h+v}$). Particles (2×10^5 particles/μL) were actuated (B = 20 mT; ω = 0.2 Hz) in a 36 μL fluid volume. (a) Sketch of the actuation process. Initially, particles are distributed over the bottom surface of the incubation chamber. By magnetic actuation, the particles are moved in a layer-like fashion upward and downward through the fluid, and during this process they form (rotating) chains. After actuation, the particles are redistributed over the surface, and the fluorescence due to the captured targets on the particle surface was measured. (b) Time dependence of the particle fluorescence relative to the background. The lines are fits based on eq 6 to determine k_a and k_d. From the fit parameters, the particle fluorescence is related to the number of bound antibodies per magnetic particle, as shown on the right axis. (c) Fitted association and dissociation rate constants for the data shown in panel b.

In particle ensembles, the proximity of particles can lead to overlapping depletion zones and therefore a further reduction in capture rates.

Target Capture by Magnetically Actuated Ensembles of Particles. In Figure 3, data is shown for different magnetic actuation protocols as well as a control without magnetic actuation. In the control experiment, particles are distributed randomly over the bottom of the incubation chamber due to sedimentation. In the case of magnetic actuation, we used gradients in the magnetic field to translate particles up and down repeatedly through the incubation chamber ($B_{grad,z}$), as sketched in Figure 3a. During this actuation, particles formed into chain-like structures oriented in the direction of the (static) magnetic field, which was in-plane with respect to the bottom surface of the incubation chamber. In addition to the translation, magnetic fields were rotated in-plane ($B_{rot,h}$) or out-of-plane ($B_{rot,v}$) to rotate the chains of particles within the local fluid.

Magnetic actuation of magnetic particles has a strong effect on the capture rate, as shown in Figure 3b. In the case of actuation, the measured curves show an initial kinetic regime and a saturation of the particle fluorescence after several tens of minutes. To fit the data, we used the following equation describing the time-dependent binding of antibodies [Ab] to a magnetic particle [MP] (see Supporting Information S5):

$$[\text{bound Ab}] = \frac{k_a[\text{MP}][\text{Ab}]}{k_a[\text{MP}] + k_d}\{1 - \exp(-(k_a[\text{MP}] + k_d)t)\} \quad (6)$$

in which k_a and k_d are, respectively, the forward and backward rate constants, or the rate constants for association and dissociation, calculated per magnetic particle. Using eq 6, we determined the association and dissociation rate constants for the different cases (Figure 3c). For the dissociation rate constant, similar values are found for the different actuation methods, with an average value of $k_d = 1.5 \pm 0.7 \times 10^{-4}$ s^{-1}. This value is consistent with the dissociation rate constant of goat IgG and protein G of $k_d \approx 1 \times 10^{-4}$ s^{-1}, as has been measured by localized surface plasmon resonance (LSPR).[11] The association rate constants, on the other hand, show a significant variation for the different types of actuation. Compared to no actuation, a field gradient of ~4 T/m (which corresponds to a single particle moving at a velocity of 12 μm/s) resulted in an increase in k_a by a factor of 8 ± 4. Combined with a rotating magnetic field, the k_a increased further. We find that out-of-plane rotating fields, with an increase in k_a of 36 ± 7 times, are more effective than in-plane rotating fields. Overall, these results clearly show that particle movement through the sample volume yields a substantial increase in the rate at which target antibodies are captured.

We attribute the observed increase in the association rate constant to the fact that local depletion zones in the target concentration are present near the particles. Such concentration gradients near the particles are generated by a transport limitation in the capture process and hence can explain why enhanced particle−fluid interaction increases capture rates. In the following paragraphs, we will discuss the underlying processes in more detail to provide further evidence for our explanation.

According to the literature, the bimolecular association of proteins (e.g., see ref 9) to antibodies is known to be generally limited by diffusive transport and not by the physicochemical reaction that finally binds the proteins. This diffusive limitation in antibody−protein association is, however, not primarily caused by the relative translational diffusion but by the relative rotational diffusion to orient the binding site of the antibody to the binding site of the protein. For example, it has been shown by Schmitz and Schurr[12] that moderate angular constraints to the relative binding site orientation decrease diffusion-controlled association rate constants by several orders of magnitude.[9] Rate constants for antibody−protein association are typically on the order of $k_a = 10^4$−10^6 M^{-1} s^{-1}.[9,11] This is small compared to the expected diffusive encounter rate based on relative translational diffusion alone, which is on the order of 10^9−10^{10} M^{-1} s^{-1} and follows from the Smoluchowski equation[13]

DOI: 10.1021/acs.analchem.6b04043
Anal. Chem. 2017, 89, 3402−3410

$$k_{diff} = 4\pi DR \quad (7)$$

with D and R being, respectively, the combined diffusivity and the encounter radius of the reacting proteins. Therefore, these low values of k_a, as typically found for antibody−protein association, will not lead to target depletion.

For the particle-based association of proteins, we find values of k_a (Figure 3c) that are much closer to the diffusive encounter rate, which we estimate at $k_{diff} = 4\pi(D_{MP} + D_{IgG})(R_{MP} + R_{IgG}) = 4.1 \times 10^{11}$ M^{-1} s^{-1}, where a hydrodynamic radius of ∼5.5 nm was used for goat IgG.[10] This constant is only a factor 6.9 ± 0.7 larger than the maximum association rate constant that we find in experiments, namely, $k_a = 6.0 \pm 0.6 \times 10^{10}$ M^{-1} s^{-1}. Clearly, for particle-based protein capture, the relative difference is much smaller as compared to antibody−protein association; consequently, a limitation by translational diffusion cannot be neglected for the association of protein targets to particles (see Supporting Information S6 for a discussion about particle-based capture versus planar capture). This is consistent with a previous study that we performed on the process of particle-based target capture. In that study, we used a model system with 200 nm particles as targets[14] and we found that the capture process is limited by both the translational and rotational diffusion of the reacting species.

The large difference between the k_a for particle-based protein association and antibody−protein association can be attributed to (i) the larger encounter radius caused by the large size of the magnetic particle and (ii) the high number of binding sites on the magnetic particle compared to a single antibody. When the surface of the magnetic particle is completely filled with binding sites, the magnetic particle can bind a target protein in almost any orientation, and during a collision with a target protein, the target protein can interact with multiple binding sites. In this way, the probability to bind is much higher for a protein encountering a magnetic particle than for a protein encountering an antibody free in solution. Thus, in the particle-based association of proteins, angular constraints for binding are weakened to such an extent that the number of encounters also becomes a limitation for the association rate.

On the basis of these arguments, we conclude that depletion layers form around the magnetic particles due to the slow translational diffusion of targets in case the magnetic particles are immobile at the bottom of the incubation chamber (see Figure 3). The depletion layers grow over time and thereby increasingly reduce the capture rate. Moving the particles through the fluid, e.g., by magnetic actuation, enhances the interaction of the particles with the fluid and thereby reduces the depletion layers around the particles. As concentration gradients are mainly developed orthogonal to the layer of particles (compare Figure 3a), both translation along the surface normal and out-of-plane rotation of magnetic particle chains are the most effective ways to reduce the concentration gradients caused by depletion.[15]

Influence of the Concentration of Magnetic Particles. Figure 4 shows how the association rate constant depends on the concentration of magnetic particles in the fluid. We applied particle concentrations below a full coverage of the surface of the incubation chamber (Figure 4a). As shown in Figure 4b, without magnetic actuation, the association rate constant k_a does not change at low particle concentrations. Above a threshold, k_a becomes smaller with increasing particle concentration. This behavior has been observed before[14] for a different experimental model system comprising 200 nm diameter fluorescent particles as targets. For low particle concentrations, it was found that the reaction reached steady state in which the concentration gradient or depletion zone around each particle is constant in time. As long as particles are sufficiently separated, i.e., at low particle concentrations, the concentration gradients or depletion zones do not overlap and k_a remains unaffected by the particle concentration. When the depletion zones overlap, i.e., at higher particle concentrations, they expand, thereby reducing k_a, until either a new steady state is obtained or until the volume is depleted of targets. From Figure 4b, we find that k_a drops starting from a concentration of ∼2×10^3 particles/μL. For a sample volume of 36 μL, sedimented particles are, on average, separated by about 20 μm. As follows from the steady-state solution of the diffusion equation for an absorbing particle,[14] at half this distance the target concentration is ∼86%. Particles that are separated by less than 20 μm, therefore, show partial overlap of their depletion zones and have a reduced association rate constant.

This effect is also observed in cases where particles are magnetically actuated (see Figure 4b). Compared to no

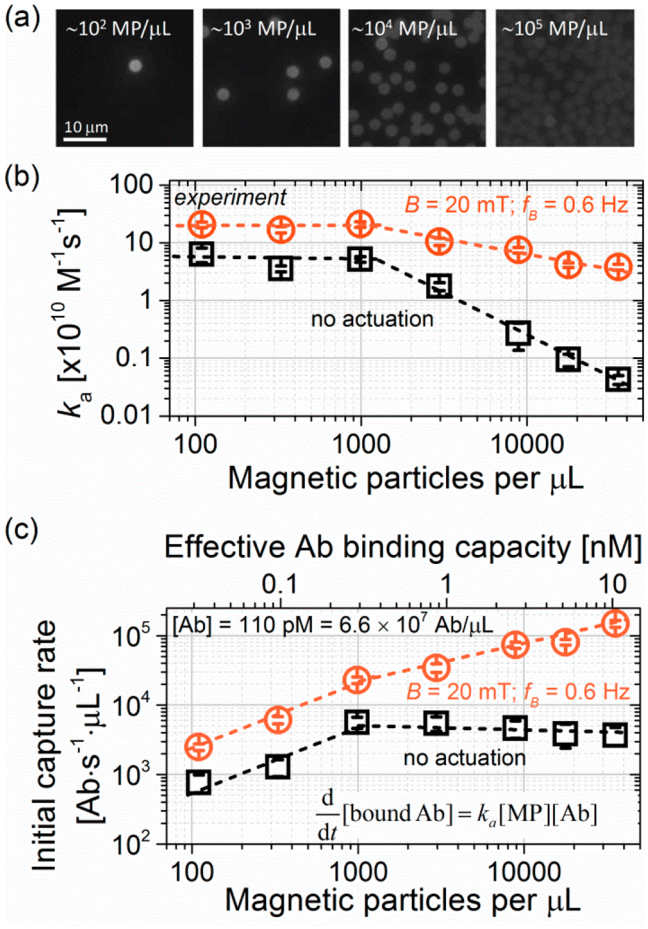

Figure 4. Experimental data on target capture by magnetically actuated ensembles of magnetic particles for varying magnetic particle concentrations. (a) Fluorescence microscopy images of magnetic particles after 30 min of incubation without actuation. (b) Experimentally determined association rate constant with and without actuation (B = 20 mT; ω = 0.6 Hz; alternated in-plane and out-of-plane rotation). Using this data, we computed (c) the antibody capture rate per μL at short times for an antibody concentration of 110 pM. The corresponding total binding capacity is plotted on the top x-axis. The dashed lines are guides to the eye.

DOI: 10.1021/acs.analchem.6b04043
Anal. Chem. 2017, 89, 3402−3410

actuation, an elevated k_a is found for all particle concentrations. Furthermore, the threshold in particle concentration above which the k_a starts to decrease is found to be the same for both cases, but the decrease is less strong in the case of magnetic actuation. The effect of magnetic actuation becomes clearer when considering the antibody capture rate at short incubation times (see Figure 4c). For low particle concentrations, the capture rate is found to increase with increasing particle concentration. As soon as the depletion zones start to overlap, no actuation leads to constant capture rates, whereas magnetic actuation enhances the capture rate with increasing particle concentration. Interestingly, the results in Figure 4c demonstrate that magnetic particle actuation achieves similar or even higher capture rates with less particles as compared to capture without actuation.

From the values of k_a in Figure 4, we quantified the increase in the target capture rate, as shown in Figure 5a. Magnetic actuation has the highest impact at high particle concentrations, when depletion is the strongest. In this regime, the capture rate can be improved by 1 to 2 orders of magnitude. For low particle concentrations, we find an increase in the capture rate of 3 ± 1 by actuating the particles, showing that movement through the fluid enhances the encounter rate also for isolated particles. Part of this increase can be attributed to the presence of a nearby surface in case of no actuation.[14] Yet the steady-state solution of the diffusion equation[13] clearly shows that individual particles form a depletion zone near their surface. In cases where the target binding probability is equal to unity during an encounter, the target concentration $c(r)$ depends on the radial distance $r \in [R, \infty)$ from the particle center as $c(r) = c(\infty)\cdot(1 - R/r)$, with R being the encounter radius of the target and the particle. For the system studied here, the binding probability is less than unity, since $k_a < k_{diff}$ (see eq 7). Consequently, depletion zones are expected to be smaller in amplitude, but enhanced particle−fluid interactions will still have a reducing effect on the depletion zones and thereby improve the capture rate.

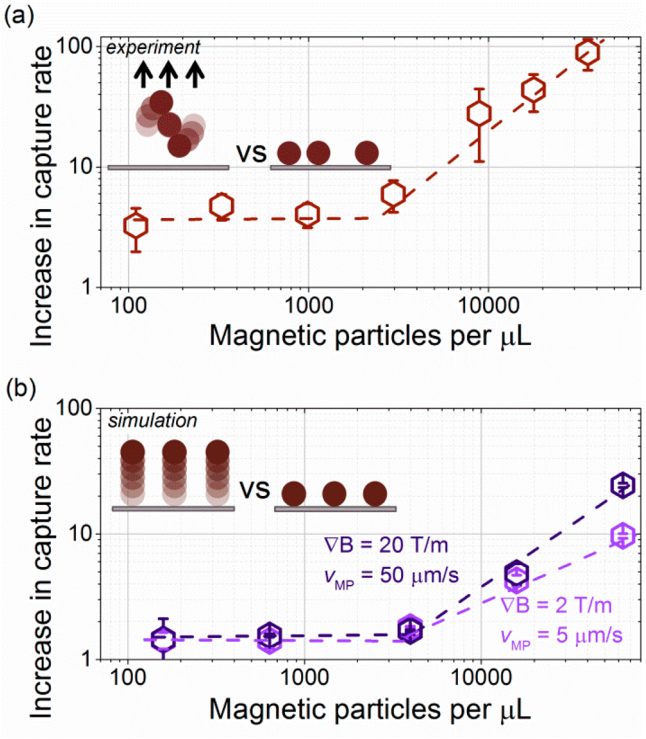

Figure 5. Relative actuation-induced increase in capture rate as found (a) in experiments on magnetically actuated ensembles of particles as shown in Figure 4, and (b) in simulations on the linear translation of single particles through the sample volume (for two different field gradients). The dashed lines are guides to the eye.

To quantitatively analyze the experimental data, target capture was simulated for different particle concentrations by varying the width of the simulated fluid cell (see Supporting Information S8). From the defined periodic boundary conditions, particles are distributed in a square lattice. Actuation of the particles consisted of a linear translation of particles upward and downward through the fluid volume, corresponding to the application of a field gradient, but without magnetic dipole−dipole interactions between the particles. As shown in Figure 5b, a similar threshold behavior is obtained in simulations as in the experimental data shown in Figure 5a. The increases in the capture rate obtained from the simulations are less than those in the experiments, as was also observed for actuation by particle translation only (see Figure 2 and related discussion). Comparing the k_a determined for (i) translation and (ii) combined translation and rotation in Figure 3c, it is found that the k_a of the combined actuation is higher by a factor of 4 ± 2. A similar difference is obtained when comparing the data in panels a and b of Figure 5. We therefore conclude that the numerical simulations confirm the increase in the capture rate by magnetic actuation.

Difference between Global and Local Mixing. It is insightful to apply the results from this work to previous work where we used magnetic fields to induce global fluid flows within a microfluidic chamber.[16] To induce such flows, no field gradients were used, but a magnetic field rotating out-of-plane with respect to the surface at a relatively high frequency (~30 Hz) was used. Such actuation applied to a high concentration of magnetic particles induces particle movement along the chamber walls, leading to a vortex type of flow within the fluid chamber. In that work, the overall reaction rate constant (i.e., $k = k_a[MP] + k_d$; see eq 6) was quantified using the same biological system as used in this work but with a larger magnetic particle diameter, namely, 10 μm. Using the findings from this work, we unravelled the association rate constant (i) for the case of induced vortical flows, $k_a = 23 \pm 4 \times 10^{10}$ M^{-1} s^{-1}, and (ii) for the case of no actuation, $k_a = 9.5 \pm 1 \times 10^{10}$ M^{-1} s^{-1}. Note that due to the larger particle diameter the diffusion rate constant is ~4 times larger, i.e., $k_{diff} = 1.5 \times 10^{12}$ M^{-1} s^{-1}, as compared to the system studied in this work.

Compared to no actuation, induced vortical flows improve k_a by a factor of 2.4, which is relatively low as compared to the improvements obtained using the actuation methods applied in this work. Part of this small improvement might be explained by the relatively low particle concentration (~4000 particles per μL), but in the experiments, the particles were locally concentrated, which would cause larger depletion layers to be formed around the particles. Another factor that affects the size of the depletion layers is the rate at which targets encounter the capture particles. Without actuation, this is controlled solely by diffusion processes. By magnetic actuation, particle−fluid interactions can be enhanced. In the induced vortical flows, the particles bring the fluid in motion and then move along with the fluid through the fluid chamber. Although global fluid mixing is achieved effectively, target capture is not effectively enhanced because encounters with the targets are still governed

DOI: 10.1021/acs.analchem.6b04043
Anal. Chem. 2017, 89, 3402−3410

mainly by diffusion within the flowing fluid. The magnetic actuation methods, as studied in this work, moved particles through the fluid without inducing global fluid flows. In this way, the fluid near the particles is refreshed rapidly, which allows targets to be brought in close proximity to the particle, reducing the depletion zones and thereby improving the capture rate.

This analysis shows that methods using (magnetic) particles that effectively induce fluid mixing are not necessarily optimal to speed up target capture. For efficient target capture, the local particle−fluid interactions need to be enhanced due to the target depletion zones that exist around capture particles.

CONCLUSIONS

The actuation of particles was investigated to achieve rapid affinity-based capture of biological targets from a fluid. Target capture is very efficient when particles are functionalized with a high density of specific binding sites on their surface. We have shown that the high density of binding sites generates depletion zones near the particles, especially at elevated particle concentrations. To maintain high capture rates, depletion can be reduced by actuating the particles, thereby enhancing particle−fluid interactions. We have shown that magnetic actuation is very effective when magnetic field gradients and rotating fields are combined in order to translate and rotate magnetic particle chains in the fluid. From experiments, we determined that magnetic actuation can increase association rate constants by up to 1 or 2 orders of magnitude. Using numerical Brownian dynamics simulations, we confirmed experimental observations and showed that detailed information can be obtained on the binding process, such as the relative orientation that is required to bind. We have also shown that optimal target capture is achieved for low Mason numbers (see Supporting Information S7) as long as the Péclet number is sufficiently high ($Pe > 1$). Lastly, for higher particle concentrations, magnetic actuation becomes increasingly more effective, as local depletion of targets plays a larger role.

Both experiments and numerical calculations show that magnetic actuation most effectively enhances target capture at high particle concentrations. However, high concentrations of particles can hinder further processing steps in an assay, like detection of the targets on the particles, for example by the formation of target-induced bonds at a sensor surface.[7] By balancing high capture kinetics with minimal hindrance of further processing steps, we assume that particle concentrations are optimal when they are not far below a full coverage of the detection surface. For such concentrations, we have shown that magnetic actuation can improve the capture kinetics by almost 2 orders of magnitude. In many reported assays based on magnetic particles,[16−18] particle concentrations are larger by at least 2 orders of magnitude compared to the highest concentration we studied here (i.e., $\sim 4 \times 10^4$ particles/μL). The application of magnetic actuation for target capture should make it possible to lower the particle concentration and reduce its negative effects while maintaining or even increasing the capture efficiency. As a result, assay performance can potentially be significantly improved.

In this study, the capture kinetics were quantified by determining association rate constants. To enable close comparison with other techniques, we believe that quantifying rate constants is the most reliable method as it allows for deep insight in the capture process. In addition, different actuation methodologies would be directly comparable if a standard assay would be used. The model system used in this study is suitable for that, as the protein G−IgG complex is well-studied and commonly used.[11,19,20] If the target molecule is already labeled, target capture can be measured in a direct way and further fluid handling steps are avoided.

Dynamic particle actuation for target capture is of particular interest for improving miniaturized bioanalytical tools. The methods can be applied not only for the capture of proteins but also for small molecules, nucleic acids, or cells. Compared to other microfluidic capture methods that require the generation of fluid flow[21−23] or mechanical movement of magnets[24] to enhance particle−fluid interactions, the magnetic actuation used in this article requires only stationary electromagnets and a current controller. In this way, an instrument−cartridge system is possible in which the instrument contains the actuation technology while the disposable cartridge can be relatively simple. We expect that the insights presented in this article on the dependence of the particle-based molecular association rate on particle velocity, density, and particle assembly characteristics will aid in the design of future bioanalytical methods and devices.

ASSOCIATED CONTENT

Supporting Information

The Supporting Information is available free of charge on the ACS Publications website at DOI: 10.1021/acs.analchem.6b04043.

(1) Field calibration of the five-pole electromagnet, (2) rotaphoresis to redistribute particles, (3) image processing to determine particle fluorescence, (4) control experiments to verify binding specificity, (5) determination of rate constants for association and dissociation, (6) comparison of particle-based capture with planar surface assays, (7) influence of field rotation parameters, (8) numerical Brownian dynamics simulations of target capture, and (9) SEM picture of M270 magnetic particles (PDF)

AUTHOR INFORMATION

Corresponding Author

*E-mail: m.w.j.prins@tue.nl.

ORCID

Arthur M. de Jong: 0000-0001-6019-7333

Menno W. J. Prins: 0000-0002-9788-7298

Present Address

[‖]Alexander van Reenen: Philips BG Emerging Businesses, Handheld Diagnostics, HTC29, 5656 AE Eindhoven, The Netherlands.

Author Contributions

The manuscript was written through contributions of all authors.

Notes

The authors declare no competing financial interest.

ACKNOWLEDGMENTS

We thank the mechanical and electronic workshops of the department of Applied Physics at Eindhoven University of Technology for manufacturing the five-pole electromagnet and the controller for the setup. This work was supported by Technology Foundation STW under Grant No. 10458.

DOI: 10.1021/acs.analchem.6b04043
Anal. Chem. 2017, 89, 3402−3410

REFERENCES

(1) Wild, D. *The Immunoassay Handbook*; Elsevier: Amsterdam, 2005.
(2) Howes, P. D.; Chandrawati, R.; Stevens, M. M. *Science* **2014**, *346*, 1247390.
(3) Vogelstein, B.; Gillespie, D. *Proc. Natl. Acad. Sci. U. S. A.* **1979**, *76*, 615−619.
(4) Boom, R.; Sol, C. J.; Salimans, M. M.; Jansen, C. L.; Wertheim-van Dillen, P. M.; van der Noordaa, J. *J. Clin. Microbiol.* **1990**, *28*, 495−503.
(5) Pickard, W. F. *J. Theor. Biol.* **2006**, *240*, 288−301.
(6) Gijs, M. A. M.; Lehmann, U.; Lacharme, F. *Chem. Rev.* **2010**, *110*, 1518−1563.
(7) Van Reenen, A.; de Jong, A. M.; den Toonder, J. M. J.; Prins, M. W. J. *Lab Chip* **2014**, *14*, 1966−1986.
(8) Van Reenen, A.; de Jong, A. M.; Prins, M. W. J. *Lab Chip* **2015**, *15*, 2864−2871.
(9) Schreiber, G.; Haran, G.; Zhou, H. X. *Chem. Rev.* **2009**, *109*, 839−860.
(10) Weiss, M.; Elsner, M.; Kartberg, F.; Nilsson, T. *Biophys. J.* **2004**, *87*, 3518−3524.
(11) Read, T.; Olkhov, R. V.; Shaw, A. M. *Phys. Chem. Chem. Phys.* **2013**, *15*, 6122−6127.
(12) Schmitz, K. S.; Schurr, J. M. *J. Phys. Chem.* **1972**, *76*, 534−545.
(13) Von Smoluchowski, M. *Z. Phys. Chem.* **1917**, *92*, 129−168.
(14) Van Reenen, A.; de Jong, A. M.; Prins, M. W. J. *J. Phys. Chem. B* **2013**, *117*, 1210−1218.
(15) Gao, Y.; van Reenen, A.; Hulsen, M. A.; de Jong, A. M.; Prins, M. W. J.; den Toonder, J. M. J. *Microfluid. Nanofluid.* **2014**, *16*, 265−274.
(16) Nam, J.-M.; Thaxton, C. S.; Mirkin, C. A. *Science* **2003**, *301*, 1884−1886.
(17) Todd, J.; Freese, B.; Lu, A.; Held, D.; Morey, J.; Livingston, R.; Goix, P. *Clin. Chem.* **2007**, *53*, 1990−1995.
(18) De Palma, R.; Reekmans, G.; Laureyn, W.; Borghs, G.; Maes, G. *Anal. Chem.* **2007**, *79*, 7540−7548.
(19) Akerstrom, B.; Bjorck, L. A. *J. Biol. Chem.* **1986**, *261*, 10240−10247.
(20) Allauzen, S.; Mani, J. C.; Granier, C.; Pau, B.; Bouanani, M. *J. Immunol. Methods* **1995**, *183*, 27−32.
(21) Lacharme, F.; Vandevyver, C.; Gijs, M. A. M. *Anal. Chem.* **2008**, *80*, 2905−2910.
(22) Moser, Y.; Lehnert, T.; Gijs, M. A. M. *Lab Chip* **2009**, *9*, 3261−3267.
(23) Kan, C. W.; Rivnak, A. J.; Campbell, T. G.; Piech, T.; Rissin, D. M.; Mösl, M.; Peterça, A.; Niederberger, H. P.; Minnehan, K. A.; Patel, P. P.; Ferrell, E. P.; Meyer, R. E.; Chang, L.; Wilson, D. H.; Fournier, D. R.; Duffy, D. C. *Lab Chip* **2012**, *12*, 977−985.
(24) Ng, A. H.; Choi, K.; Luoma, R. P.; Robinson, J. M.; Wheeler, A. R. *Anal. Chem.* **2012**, *84*, 8805−8812.

DOI: 10.1021/acs.analchem.6b04043
Anal. Chem. 2017, 89, 3402−3410